Chemical Geology 584 (2021) 120505

Contents lists available at ScienceDirect

Chemical Geology

journal homepage: www.elsevier.com/locate/chemgeo

Oceanic mercury recycled into the mantle: Evidence from positive Δ^{199}Hg in lamprophyres

Xueyun Wang [a,b], Changzhou Deng [a], Zongyong Yang [a], Jing-Jing Zhu [a,*], Runsheng Yin [a,*]

[a] State Key Laboratory of Ore Deposit Geochemistry, Institute of Geochemistry, Chinese Academy of Sciences, Guiyang 550081, China
[b] University of Chinese Academy of Sciences, Beijing 100049, China

ARTICLE INFO

Editor: Dr. Oleg Pokrovsky

Keywords:
Hg isotopes
Mantle
Lamprophyre
Subduction
Marine Hg recycling

ABSTRACT

Due to mercury (Hg) is a global pollutant, the biogeochemistry of Hg in Earth's surface environment has been well studied. However, the cycling of Hg in interior reservoirs remains less clear, limiting our understanding of the global Hg geochemical cycle. Here, we use Hg isotopes to constrain the sources of Hg in typical alkaline lamprophyres in South China: the Early Ordovician lamprophyres in the Zhenyuan area and the Late Cretaceous lamprophyres in the Zhenfeng area. Lamprophyres from both areas are enriched in large-ion-lithophile elements (LILEs) and light rare earth elements (LREEs) but depleted in high-field-strength elements (HSFEs), typical of subduction-related igneous rocks. The Early Ordovician and Late Cretaceous lamprophyres show significantly positive to near-zero Δ^{199}Hg values of 0.18 to 0.37‰ and − 0.08 to 0.36‰, respectively. The positive Δ^{199}Hg values are consistent with that reported for marine sediments and seawaters, suggesting Hg in these lamprophyres was sourced from marine reservoirs. This study suggests a heterogeneous distribution of Hg in the mantle and demonstrates that subducted marine materials can have contributed a substantial amount of Hg into the mantle.

1. Introduction

Mercury (Hg) is a globally distributed heavy metal pollutant, with multiple physical states (gaseous, liquid, and solid) and oxidation states (0, +1, and + 2) in nature. Mercury is released to the environment through natural (e.g., volcanism) and anthropogenic sources (e.g., fossil fuel combustion, nonferrous metal refining), mainly in the form of gaseous Hg(0)(Pirrone et al., 2009). Gaseous Hg(0) has a lifetime of 1 year in the atmosphere, allowing the global transport and deposition to the land and ocean ecosystems (Selin, 2009). Owing to its extreme toxicity and mobility, the geochemical fate of Hg in Earth's surface reservoirs (e.g., atmosphere, soil, sediments, biosphere) has been well studied (Selin, 2009). In the preindustrial era, when anthropogenic Hg emission was not significant, volcanism served as the major natural source of Hg in the surface environment (Sherman et al., 2009; Zambardi et al., 2009). However, to date, the deep cycle of Hg on Earth, in particular, the sources and isotopic composition of Hg in deep reservoirs (e.g., crust and mantle), remain poorly understood.

Mercury isotope geochemistry is a newly developed tool for constraining the sources and fates of Hg in the environment. The seven natural stable isotopes of Hg (^{196}Hg, ^{198}Hg, ^{199}Hg, ^{200}Hg, ^{201}Hg, ^{202}Hg, ^{204}Hg) can undergo both mass-dependent fractionation (MDF, expressed as δ^{202}Hg) and mass-independent fractionation (MIF) of the odd-mass isotopes (expressed as Δ^{199}Hg) and the even-mass isotopes (expressed as Δ^{200}Hg). Hg-MDF is ubiquitous and occurs during all biological, chemical, and physical processes (Blum et al., 2014; Kwon et al., 2020). Hg even-MIF is detected mainly in atmospherically-derived samples (e.g., rainfall) and rarely reported in other reservoirs (Kwon et al., 2020). Odd-MIF mainly occurs during photochemical processes with little contribution from other reactions and therefore provides clear source constraints (Blum et al., 2014; Kwon et al., 2020). A large extent of Δ^{199}Hg (−6.0 to 6.0‰) was reported in Earth's surface reservoirs, with positive Δ^{199}Hg in marine reservoirs (e.g., marine sediments, seawater, and fish) and negative Δ^{199}Hg in terrestrial reservoirs (e.g., soil and vegetation) (Blum et al., 2014 and references therein). In comparison, studies on a few igneous rocks showed a small extent of Hg-MIF (Δ^{199}Hg: 0 ± 0.1‰, 2SD) (Smith et al., 2008; Moynier et al., 2020), indicating Earth's deep reservoirs (crust and mantle) lack significant Hg-MIF due to the absence of photochemical reactions. A recent study, however, reported positive Δ^{199}Hg (−0.3 to 0.4‰) in hydrothermal ore deposits at active continental margin settings (Deng et al., 2021), implying that Hg from surface reservoirs may be involved in deep cycling through

* Corresponding authors.
E-mail addresses: zhujingjing@mail.gyig.ac.cn (J.-J. Zhu), yinrunsheng@mail.gyig.ac.cn (R. Yin).

https://doi.org/10.1016/j.chemgeo.2021.120505
Received 6 June 2021; Received in revised form 16 August 2021; Accepted 24 August 2021
Available online 26 August 2021

subduction of oceanic plates carrying marine sediments.

Mantle-derived magmatic rocks are common proxies in deciphering the geochemical characteristics of the mantle. Growing evidence from Sr-Nb-Pb-Hf isotopes show mantle heterogeneity and suggest the involvement of crustal materials into the mantle via plate subduction (Hofmann, 2003; Anderson, 2006). Lamprophyre represents a rare and peculiar mantle-derived rock type (Bergman, 1987), characterized by mainly ultramafic compositions and high abundances of volatiles (e.g., H_2O, CO_2, halogens; Rock, 1991). The basic magma of lamprophyres has a low viscosity and a fast ascent rate, so the degree and chance of being contaminated by the crust during the ascent process are both small (Zhou et al., 1998). Lamprophyres are commonly characterized by a panidiomorphic porphyritic texture carrying hydrous mafic phenocrysts, which may represent primary mantle-derived magmas (Su et al., 2017). Some lamprophyres also show the enrichment of K-bearing and other incompatible element-enriched minerals (e.g., phlogopite, K-richterite, apatite), suggesting that they were formed as a consequence of the mantle metasomatism by fluids and melts probably derived from the oceanic plate subduction (Xiang et al., 2018).

Late Cretaceous and Early Ordovician lamprophyre dikes occur in the Yangtze Block, South China (Su, 2002; Liu et al., 2010; Xiang et al., 2020). Geochemical evidence, e. g., whole-rock elemental and Sr-Nd-Hf isotopes collectively suggest the alkaline lamprophyres in South China are sourced from the metasomatized lithospheric mantle (Su, 2002; Chen et al., 2009; Xiang et al., 2018). A study on the Hg isotopic composition of these lamprophyres may provide insights into the geochemical cycling of Hg in the mantle. Here, we carried out the first study on the Hg isotopic composition of the Late Cretaceous and Early Ordovician lamprophyres in Guizhou Province, South China, to understand their Hg sources. Combined with major and trace elements data, we demonstrate that the subduction of marine materials (sediments and seawater) contributed a substantial amount of Hg into the mantle.

2. Geological background

The Yangtze Block, located in South China, is adjacent to the North China Craton in the north, the Songpan Ganzi block in the northwest, the Cathaysian Block in the southeast, and the Indosinian plate in the southwest (Fig. 1a). The area subsided to form a large basin with the Caledonian tectonic cycle during Devonian to Triassic, which is now composed of Devonian, Carboniferous, Permian, and Triassic sedimentary strata (Liu et al., 2010).

Numerous alkaline ultramafic dikes, which mainly consist of lamprophyres, are distributed in the Yangtze Block (e.g., Zhenfeng and Zhenyuan; Fig. 1a). Alkaline ultramafic dikes in the Zhenfeng area, which are mainly intruded into Triassic strata (Fig. 1b) and have zircon U—Pb and phlogopite $^{40}Ar/^{39}Ar$ ages of ~88–85 Ma, were previously defined as lamprophyre by Su et al. (2009) or pyroxenite by Liu et al. (2010). We support Su et al. (2009) because the Zhenfeng samples have porphyritic textures and abundant phlogopite phenocrysts (Fig. 2), which are typical features of lamprophyres but never exist in pyroxenite. In the Zhenyuan area (Fig. 1c), the Early Ordovician lamprophyre dikes are mainly intruded into Cambrian strata. The apatite from the Zhenyuan lamprophyres was dated at 473 ± 21 Ma (Li et al., 2016). A recent study demonstrated that ocean slab subduction beneath the southeastern margin of the Yangtze Block during Neoproterozoic played a crucial role in the formation of the Zhenyuan dikes (Xiang et al., 2018).

Fresh lamprophyre samples were collected from one ultramafic dike (Baifen) in Zhenyuan (Fig. 1c) and five ultramafic dikes (Bianjiao, Yangjiazhai, Yinhe, and Lurong and Baiceng) in Zhenfeng (Fig. 1b). The widths of these dikes range from 1.0 to 8.0 m and the length from 30 m to 1 km. In the laboratory, any weathering layers were cut off. A further microscope observation demonstrated limited or no secondary alteration in the collected samples (Fig. 2). The lamprophyre samples are strongly porphyritic with phenocrysts of phlogopite and diopside. The

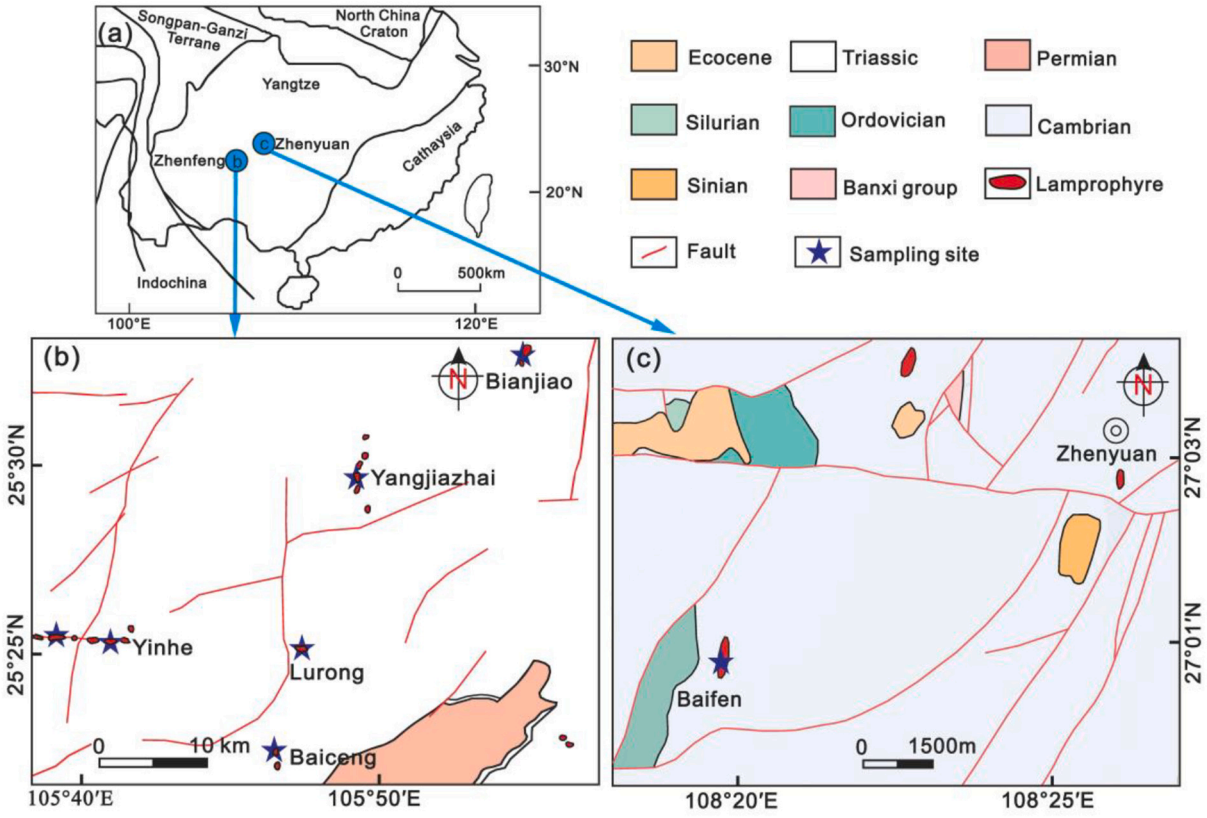

Fig. 1. (**a**) Geological framework of South China Block (after Xiang et al., 2020). (**b**) Simplified geological distribution of the studied lamprophyre dikes in the Zhenfeng area. (**c**) Simplified geological distribution of the studied lamprophyre dikes in the Zhenyuan area.

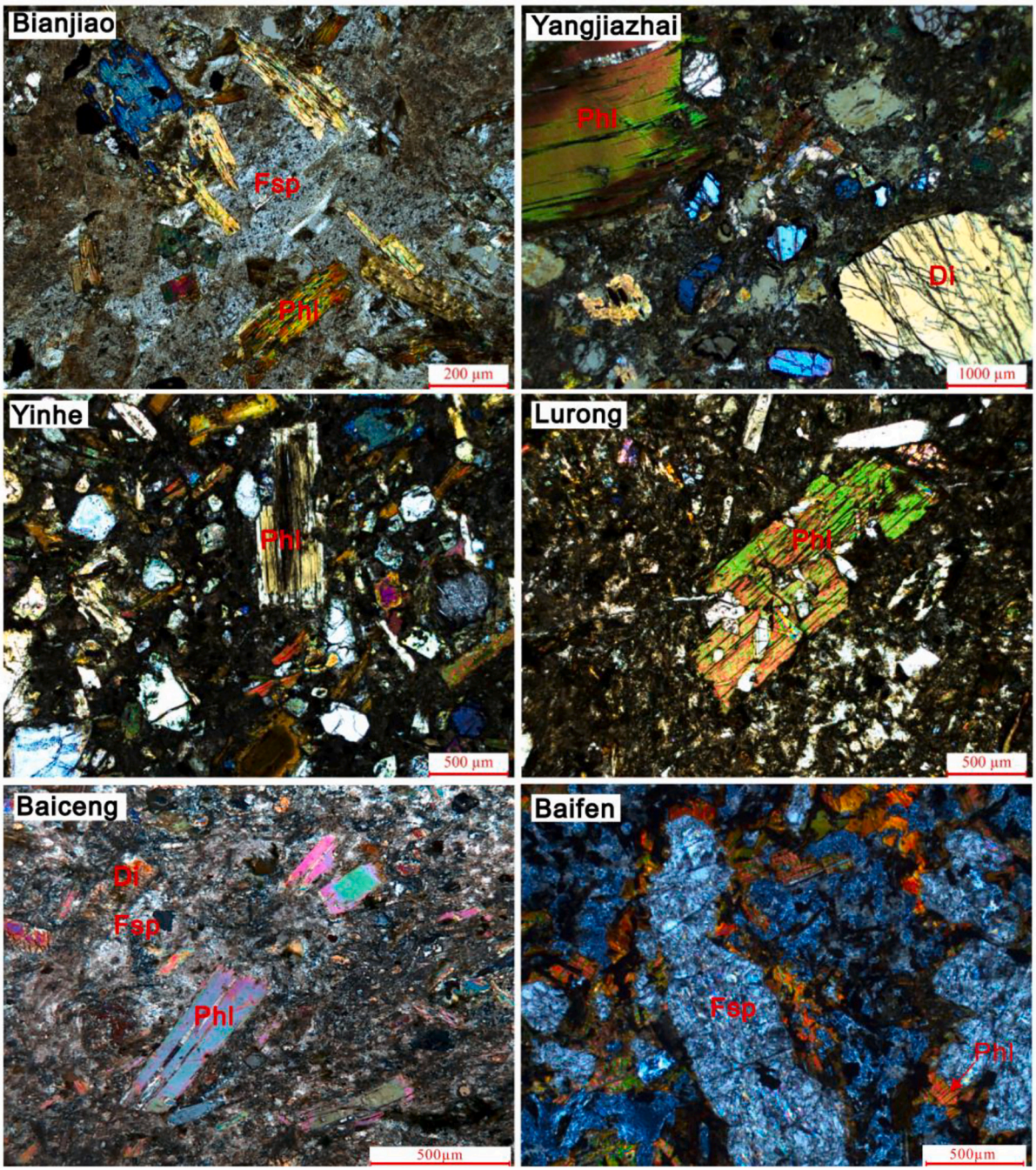

Fig. 2. Representative photomicrographs showing the petrographic features of the studied lamprophyre samples. Di diopside, Fsp feldspar, Ol olivine, Phl phlogopite.

groundmass consists of phlogopite, diopside, and minor feldspar (Fig. 2).

3. Analytical methods

The samples (17 from Zhenfeng and 13 from Zhenyuan) were pre-cleaned with 18.2 MΩ·cm water and air-dried in the laboratory. The samples were powdered and homogenized for major and trace elements, and Hg isotope analysis. Major and trace elements were analyzed at the ALS Minerals-ALS Chemex, Guangzhou, China, using PANalytical PW2424 X-ray fluorescence spectrometer and Agilent 7900 inductively coupled plasma-mass spectrometry, respectively. The analytical uncertainties for major and trace element analysis were both within 5%.

Total Hg (THg) concentration and Hg isotopic composition were measured at the Institute of Geochemistry, Chinese Academy of Sciences (IGCAS). THg concentration was determined by the Lumex RA-915+ Hg analyzer coupled with a PYRO-915+ attachment (Russia), yielding Hg recoveries of 90–110% for GSS-4 (soil) standard reference material (SRM) and uncertainty of <10% for sample duplicates. Another SRM BHVO-2 (basalt) was also measured, showing THg concentration of 5.7 ± 0.4 ng/g (n = 3), which is similar to previously reported values (6.0 ng/g, Geng et al., 2018). A double-stage tube furnace coupled with 5 mL of 40% acid mixture (HNO_3/HCl = 2/1, v/v) was used for preconcentration of Hg for isotope analysis (Zerkle et al., 2020). According to the measured THg concentrations, proper amounts of each sample containing 10 ng Hg were weighed for Hg preconcentration. The preconcentrated solutions were diluted to 0.5 ng/mL Hg in 10–20% acid

and measured using a Neptune Plus multi-collector inductively coupled plasma mass spectrometer (MC-ICP-MS), following a previous method (Yin et al., 2016). THg concentrations of the measured solutions were 0.43–0.55 ng/mL, according to the ^{202}Hg signals of MC-ICP-MS. In other words, the preconcentration method yielded Hg recoveries of 86–110% for samples. The Hg blank in the trapping solutions was <50 pg, less than 0.5% of the Hg in the sample solutions.

Hg isotope ratios were reported following convention (Blum and Bergquist, 2007). Briefly, MDF is expressed in δ^{202}Hg notation in units of ‰ referenced to the NIST-3133 Hg standard (analyzed before and after each sample):

$$\delta^{202}\mathrm{Hg}(‰) = \left[\left(^{202}\mathrm{Hg}/^{198}\mathrm{Hg}_{\mathrm{sample}}\right)/\left(^{202}\mathrm{Hg}/^{198}\mathrm{Hg}_{\mathrm{standard}}\right) - 1\right] \times 1000$$

MIF is reported in Δ notation, which describes the difference between the measured δ^{xxx}Hg and the theoretically predicted δ^{xxx}Hg value, in units of ‰:

$$\Delta^{xxx}\mathrm{Hg} = \delta^{xxx}\mathrm{Hg} - \delta^{202}\mathrm{Hg} \times \beta$$

β is 0.252 for ^{199}Hg, 0.5024 for ^{200}Hg, and 0.752 for ^{201}Hg. Hg concentrations and acid matrices in the bracketing NIST-3133 solutions were matched with neighboring samples. NIST-3177 secondary standard solutions, diluted to 0.5 ng/mL Hg with 10% HCl, were measured every 10 samples. The overall average and uncertainty of NIST-3177 (δ^{202}Hg: −0.53 ± 0.12‰; Δ^{199}Hg: −0.01 ± 0.06‰; Δ^{200}Hg: −0.03 ± 0.05‰; Δ^{201}Hg: −0.02 ± 0.06‰; 2SD, n = 3), GSS-4 (δ^{202}Hg: −1.69 ± 0.11‰; Δ^{199}Hg: −0.37 ± 0.06‰; Δ^{200}Hg: −0.04 ± 0.04‰; Δ^{201}Hg: −0.39 ± 0.06‰; 2SD, n = 3) and BHVO-2 (δ^{202}Hg: −2.11 ± 0.12‰; Δ^{199}Hg: −0.04 ± 0.07‰; Δ^{200}Hg: −0.00 ± 0.06‰; Δ^{201}Hg: 0.01 ± 0.06‰; 2SD, n = 3) agree well with previous results (Blum and Bergquist, 2007; Deng et al., 2021; Geng et al., 2018). The largest values of standard deviation (2SD) for NIST-3177, GSS-4, and BHVO-2 are used to reflect analytical uncertainties.

4. Results

Major and trace elemental data are presented in **Table S1**. The Zhenfeng samples show SiO_2 contents of 30.3–53.2 wt%, MgO of 4.88–13.2 wt%, Cr of 80.0–640 ppm, and Ni of 13.4–153 ppm. The Zhenyuan samples show SiO_2 contents of 37.7–45.9 wt%, MgO of 8.86–13.6 wt%, Cr of 570–700 ppm, and Ni of 509–568 ppm. On the Nb/Y vs. Zr/TiO_2 diagram (Fig. 3), all samples are plotted in the alkaline series field with characteristics of low Zr/TiO_2 ratios and high Nb/Y ratios. All lamprophyre samples display coherent chondrite-normalized rare earth element (REE) patterns, with light rare earth elements (LREEs) enrichment and fractionated REEs (**Fig. 4a** and **c**). In the primitive mantle normalized multi-element variation diagram (Fig. 4 **b** and **4d**), the five dikes are significantly enriched in large ion lithophile elements (LILEs, e.g., Ba and Rb) and depleted in high-field-strength elements (HSFEs, e.g., Nb, Zr, and Ti). All the samples show high and variable weight loss on ignition (LOI, 2.22–15.3 wt%), similar to previous results for lamprophyres worldwide (2–12 wt%; Owen, 2008; Hauser et al., 2010; Liu et al., 2010; Aghazadeh et al., 2015).

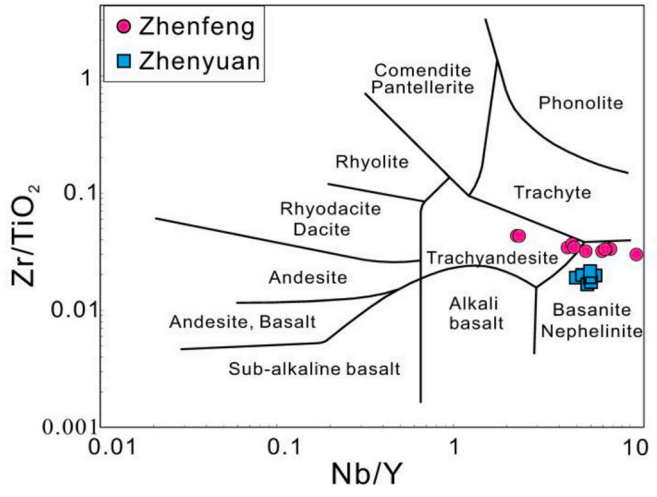

Fig. 3. Plots of Zr/TiO_2 vs. Nb/Y of lamprophyre samples from Zhenyuan and Zhenfeng in Guizhou (after Winchester and Floyd, 1977).

The THg concentration and Hg isotopic composition of the samples are given in **Table S2**. All the lamprophyre samples show large variations of THg concentrations (1.12 to 19.5 ppb) and Hg isotopic ratios (δ^{202}Hg: −5.24 to −0.10‰; Δ^{199}Hg: −0.08 to 0.40‰), suggesting a heterogeneous distribution of Hg in the mantle reservoir. Specifically, the Zhenfeng and Zhenyuan samples show δ^{202}Hg of −3.72 to −0.10‰ and − 5.24 to −1.94‰, respectively. Most of these values are similar to previous results on volcanic rocks (−4 to 0‰, Smith et al., 2008; Moynier et al., 2020), except for two samples from Zhenyuan showing more negative δ^{202}Hg of < −4‰. Most of the Zhenfeng samples show near-zero Δ^{199}Hg (−0.08 to 0.08‰), which are consistent with previous studies that reported Δ^{199}Hg of 0 ± 0.1‰ (SD) in igneous rocks (Smith et al., 2008; Moynier et al., 2020). However, four samples from Zhenfeng and all the samples from Zhenyuan show significantly positive Δ^{199}Hg (0.18 to 0.40‰), with a Δ^{199}Hg/Δ^{201}Hg ratio of 1.04, consistent with that observed during photochemical reduction of aqueous Hg(II) (Δ^{199}Hg/Δ^{201}Hg = 1.0 to 1.3, Bergquist and Blum, 2007; Zheng and Hintelmann, 2009).

5. Discussion

Post-magmatic alteration should be considered before probing into their petrogenesis. The high and variable LOI values (2.22–15.3 wt%) might be related to secondary alteration, which results in high volatile contents (Williams et al., 2004). However, fresh lamprophyres could also show high LOI values (2–12 wt%), due to auto-metasomatism (Owen, 2008; Hauser et al., 2010; Liu et al., 2010; Aghazadeh et al., 2015), reflected by abundant hydrous minerals (e.g., phlogopite). Most of the samples show LOI values of <10 wt%, and are characterized by (i) the absence of secondary minerals under microscope observation (Fig. 2), (ii) a lack of correlation between LOI and major (e.g., K_2O, Na_2O) and mobile trace elements (e.g., Ba, Rb) ($p > 0.05$, *t-test*), and (iii) positive correlations between immobile Zr and mobile LILEs (e.g., K, Ba; $p < 0.05$, *t-test*), which collectively ruled out post-magmatic alteration. Only two samples from Zhenfeng and four samples from Zhenyuan are characterized by high LOI values of >10 wt% (**Table S1**), which may be a result of secondary alteration. To avoid misinterpretation, these samples with LOI of >10 wt% are not added to the plots of Figs. 5-6 and will not be discussed below.

The lamprophyre samples are enriched in LILEs and depleted in HFSEs (Fig. 4), and show high Th/Yb and Ta/Yb ratios (Fig. 5a), suggesting that they were derived from an enriched mantle source modified by slab subduction (Elliott, 2004). This can be supported by the previously observed relatively radiogenic Nd isotope feature in Zhenfeng lamprophyres (Liu et al., 2010). Compared to mid-ocean ridge basalts (MORBs), all the investigated samples show much higher Ba/Nb and Th/Nb ratios (Fig. 5b), suggesting that mantle metasomatism by slab-derived fluid or sediment melt could have been involved. Notably, compared to the Zhenyuan samples, those from Zhenfeng show higher Cs/Nb but lower Nb/Th ratios (Fig. 5c), suggesting relatively higher degrees of fluid metasomatism.

The THg concentrations (1.12 to 10.2 ppb) of the investigated lamprophyres with LOI of <10 wt% are higher than that estimated for the primitive mantle (0.4 to 0.6 ppb, Canil et al., 2015), indicating (1) additional processes that enrich Hg in lamprophyres or (2) some extra Hg was added into the mantle. However, since Hg and its compounds are highly volatile, Hg tends to escape from the magma and release to the

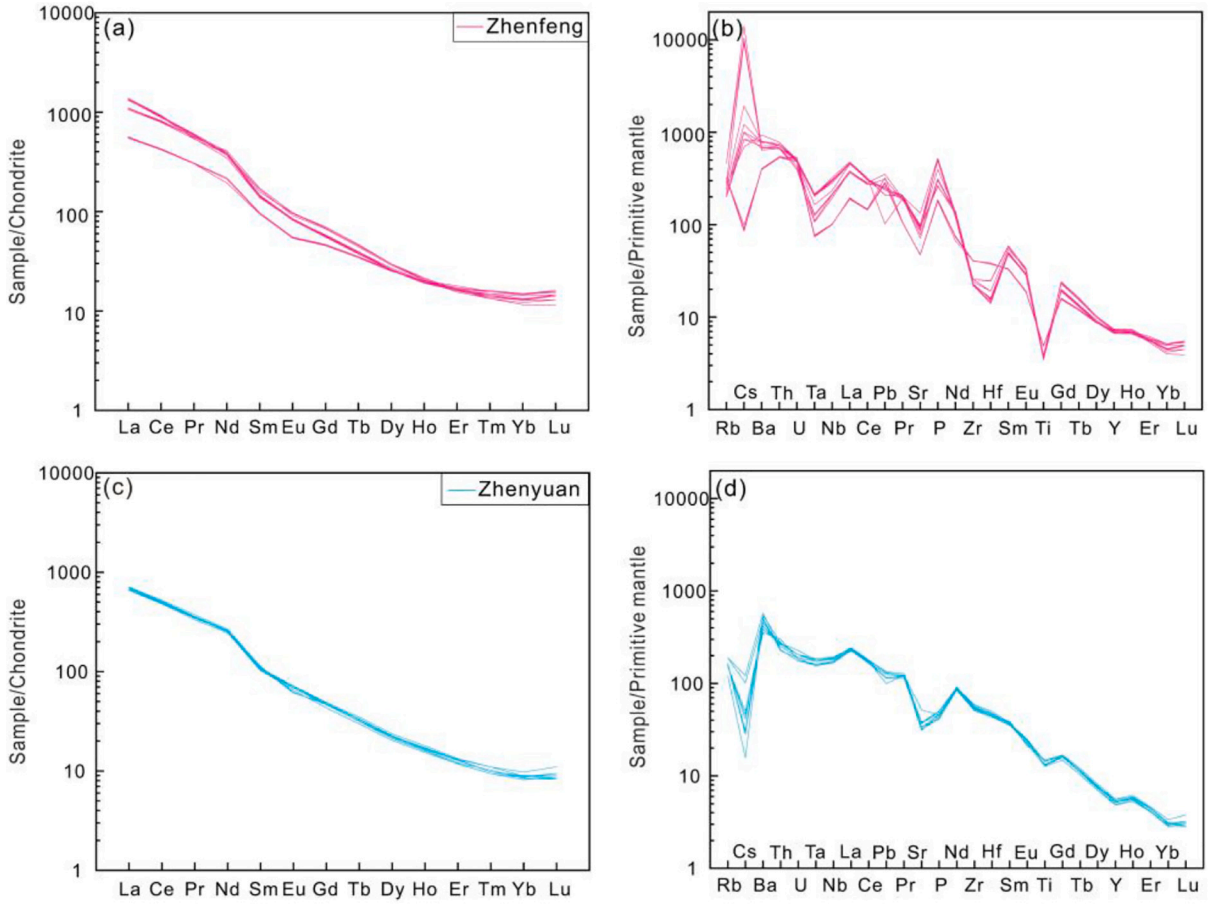

Fig. 4. Chondrite-normalized rare earth element patterns (**a**) (**c**) and primitive mantle-normalized spider diagrams (**b**) (**d**) of lamprophyre samples collected from Zhenfeng and Zhenyuan. REE abundances for chondrites and trace element abundances for primitive mantle are after Sun and McDonough (1989).

surface environment through the degassing of Hg from deep reservoirs at plate boundaries and intraplate settings (e.g., volcanoes, hot spots, and oceanic spreading centers) (Sherman et al., 2009), it is unlikely Hg can be enriched in the lamprophyres during magmatic processes.

The large variation of Hg isotopes (δ^{202}Hg: −4.38 to −0.10‰; Δ^{199}Hg: −0.08 to 0.37‰) in the lamprophyre samples with LOI of <10 wt%, as shown in Fig. 6a, more likely reflects the source variation of Hg. In previous studies, δ^{202}Hg has been used as a tracer to constrain the sources of Hg in natural samples. However, the variation of δ^{202}Hg is also a function of a large number of physical, chemical, and biological processes that induce Hg-MDF (Blum et al., 2014 and references therein). Magmatic processes may cause large Hg-MDF, as a large variation of ~4‰ in δ^{202}Hg has been observed in magmatic rocks (Smith et al., 2008; Moynier et al., 2020). Studies have also demonstrated a δ^{202}Hg variation of ~5‰ in hydrothermal deposits, suggesting Hg-MDF may occur during hydrothermal processes (e.g., oxidation, fluid boiling and mineral precipitation) (Smith et al., 2005; Smith et al., 2008). Nevertheless, due to the lack of complete understanding of all these Hg-MDF processes in deep reservoirs, we find that δ^{202}Hg is not considered to be completely diagnostic of Hg sources. Instead, we focus on the Hg-MIF signal as a source tracer, as discussed below.

Hg-MIF provides direct constraints on the sources of Hg in these samples, as it mainly occurs during photochemical processes with little contribution from other reactions. Significant Hg-MIF, with Δ^{199}Hg/Δ^{201}Hg ratios of 1.0 to 1.3 (Fig. 6a), has been observed in Earth's surface reservoirs (e.g., soil, plants, seawater, and marine sediments). Aqueous Hg(II) photoreduction, which generates Δ^{199}Hg/Δ^{201}Hg ratios of 1.0 to 1.3 (Bergquist and Blum, 2007; Zheng and Hintelmann, 2009), is the major driving force of the Hg-MIF in natural samples (Blum et al., 2014 and references therein). Magmatic processes and hydrothermal processes have been previously suggested to not trigger Hg-MIF (Smith et al., 2008; Moynier et al., 2020). It has been generally assumed that Earth's interior lacks significant Hg-MIF, due to the absence of photochemical reactions (Blum et al., 2014). As shown in Fig. 6b, all the Zhenyuan samples and four Zhenfeng samples show significantly positive Δ^{199}Hg (0.18 to 0.40‰) with Δ^{199}Hg/Δ^{201}Hg of 1.04, which are in line with that observed during photochemical reduction of aqueous Hg (II) and in Earth's surface reservoirs, suggesting that Hg in surface reservoirs may have been recycled into the mantle through plate tectonics.

Aqueous Hg(II) photoreduction occurs in Earth's surface environment, leading to negative Δ^{199}Hg in the product gaseous Hg(0), and positive Δ^{199}Hg in the residual Hg(II) phase (Bergquist and Blum, 2007; Zheng and Hintelmann, 2009). Consequently, terrestrial vegetation mainly shows negative Δ^{199}Hg (−0.6 to 0‰, Fig. 6), due to the primary accumulation of Hg(0) during foliage uptake (Demers et al., 2013). The Ordovician period experienced the first appearance of non-vascular plants like mosses and liverworts (Lenton et al., 2012), and these plant species have been demonstrated to also accumulate atmospheric Hg(0) and have negative Δ^{199}Hg (Carignan et al., 2009). Soil receives a substantial amount of Hg from litterfall (Biswas et al., 2008; Demers et al., 2013; Jiskra et al., 2017), and therefore is also characterized by negative Δ^{199}Hg (−0.6 to 0‰, Fig. 6). The ocean reservoir mainly receives Hg through wet deposition of Hg(II), therefore resulting in positive Δ^{199}Hg observed in modern seawater (0.1 to 0.3‰, Štrok et al., 2015) and marine sediments (0 to 0.4‰, Yin et al., 2015). By analogy, we expect ancient marine sediments would also have positive Δ^{199}Hg, which can be supported by the positive Δ^{199}Hg observed in paleo-sediments deposited in the Early Cambrian and Late Permian oceans (Yin et al.,

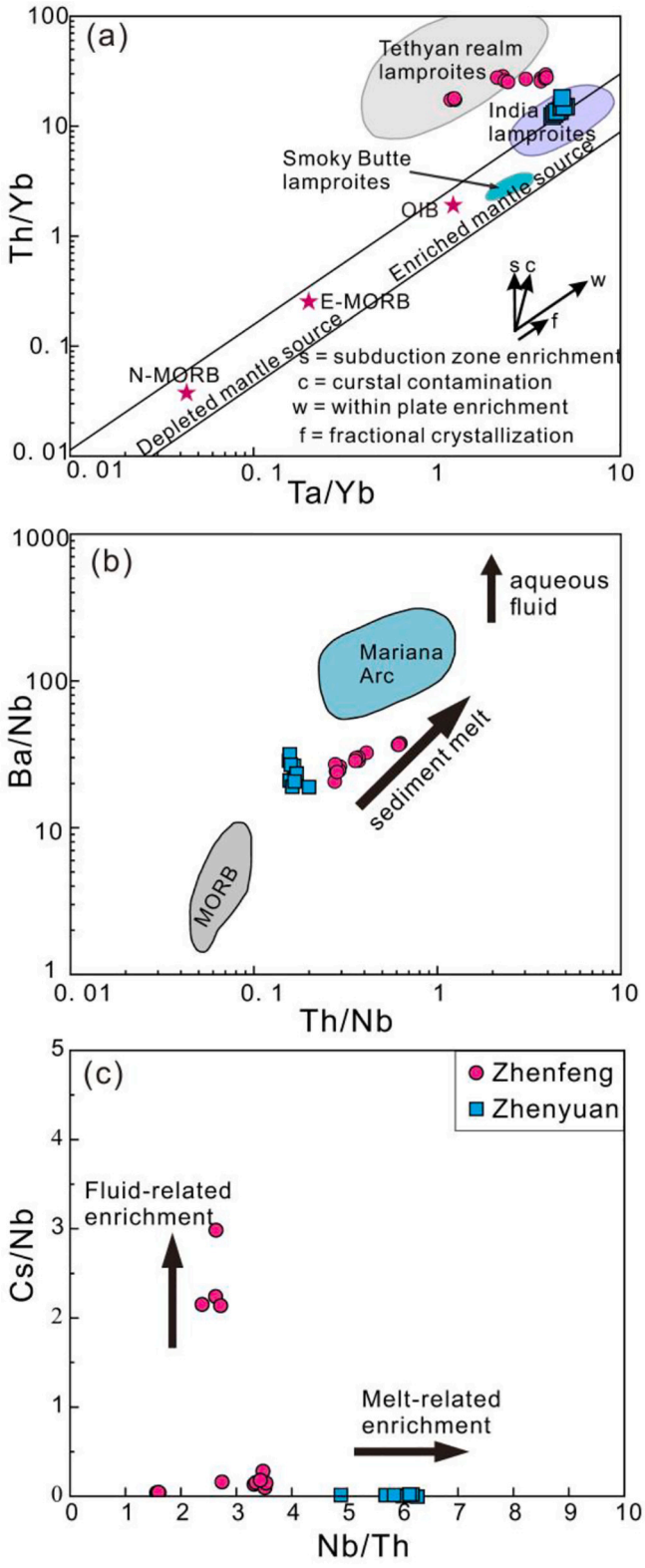

Fig. 5. Plots of Th/Yb vs. Ta/Yb (a) to characterize the magma source, Ba/Nb vs. Th/Nb (b) to show the deep sediment-derived melt and the aqueous fluid, and Cs/Nb vs. Nb/Th (c) to confirm whether it is related to melt-related or fluid-related enrichment. Data of N-MORB, *E*-MORB, and OIB are from Sun and McDonough (1989). Data of Tethyan realm, India, and Smoky Butte lamproites are from Lustrino et al. (2016) and references therein. Data of MORB composition, Mariana arc are from Pearce et al. (2005) and Stern et al. (2013), respectively.

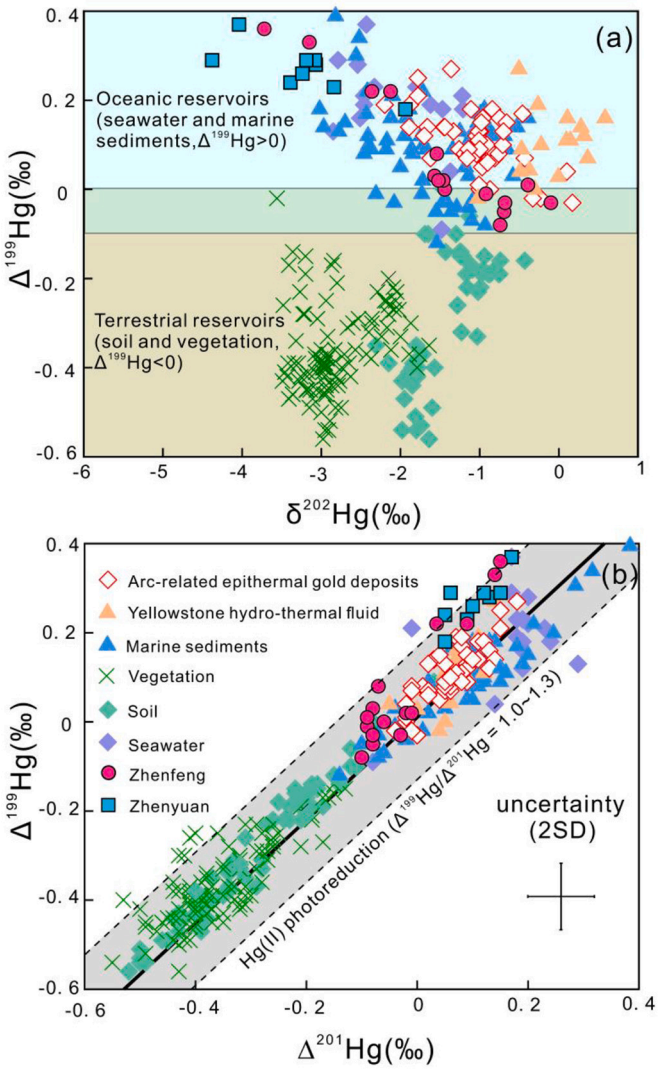

Fig. 6. Plots of Δ^{199}Hg versus δ^{202}Hg (a) and Δ^{199}Hg versus Δ^{201}Hg (b) for lamprophyre samples collected from Zhenyuan and Zhenfeng, soil (Biswas et al., 2008; Demers et al., 2013; Zheng et al., 2016; Jiskra et al., 2017), vegetation (Demers et al., 2013; Yu et al., 2016), seawater (Štrok et al., 2015), marine sediments (Yin et al., 2015; Yin et al., 2017; Grasby et al., 2017), arc-related low-temperature hydrothermal deposits (Deng et al., 2021), and hot spring fluid and precipitate samples from the Yellowstone Plateau volcanic field, USA (Sherman et al., 2009).

2017; Grasby et al., 2017, Fig. 6). The positive Hg-MIF observed in our lamprophyre samples implies that subduction of oceanic plates carrying seawater and marine sediments may have contributed substantial amounts of Hg into the mantle. This is supported by a previous study by Xiang et al. (2018), which demonstrated the enrichment of K-bearing and other incompatible element-enriched minerals (e.g., phlogopite, K-richterite, apatite) in some lamprophyre dikes in South China (e.g., Zhenyuan), and suggested that that ocean slab subduction beneath the southeastern margin of the Yangtze Block during Neoproterozoic played a crucial role in the formation of these dikes (Xiang et al., 2018). Since Hg is highly volatile, Hg may be released from the subduction-derived oceanic fluids or melts to the mantle source of lamprophyres. Consistent with our study, a previous study observed positive Δ^{199}Hg (0.06 to 0.27‰; Fig. 6b) in fluid and sinter samples from Ojo Caliente hot spring in the Yellowstone Plateau volcanic fields (Sherman et al., 2009). The positive Δ^{199}Hg in the Yellowstone Plateau volcanic field may be explained by upwelling asthenospheric mantle flow induced by the subducting Pacific plate (Kincaid et al., 2013). A recent study by Deng

et al. (2021) reported positive Δ^{199}Hg in arc-related low-temperature hydrothermal deposits (−0.02 to 0.27‰; Fig. 6b), and the positive Δ^{199}Hg was attributed to the subduction of marine sediments.

Regarding our samples, one may wonder that the Hg-MIF was predominately caused by secondary alteration by meteoric water. However, this is unlikely for the lamprophyre samples with LOI of less than 10 wt %, given their consistently low Hg concentrations and a lack of correlation between LOI and Hg ($p > 0.05$, *t-test*). Meanwhile, meteoric waters (e.g., precipitation) contain very low Hg levels (0.35–11 ng/L, Chen et al., 2012) with positive Δ^{200}Hg (0.21 to 1.24‰). The four lamprophyre samples from the Zhenfeng area and all samples from the Zhenyuan area with significantly positive Δ^{199}Hg only show slightly positive Δ^{200}Hg (0.03 to 0.11‰, **Table S2**), suggesting water-rock interaction was not a sole driver for the Δ^{199}Hg in our lamprophyre samples. It is also possible that the lamprophyre magma was affected by Hg of country rocks, such as marine sedimentary strata which has positive Δ^{199}Hg, however, a lack of significant correlation between Δ^{199}Hg and Nb/La and MgO in our samples ($p > 0.05$, t-test) suggests crustal contamination is of less importance to the observed Hg-MIF. Previous studies also precluded crustal contamination in the Zhenfeng and Zhenyuan lamprophyres, based on their homogeneous Sr-Nd-Hf isotope ratios (Su, 2002; Xiang et al., 2020).

Overall, we suggest that subducted marine materials (e.g., seawater and sediments) are responsible for the observed positive Δ^{199}Hg in our lamprophyre samples. Our study demonstrates mantle Hg isotope heterogeneity and reveals large-scale translithospheric Hg recycling via plate tectonics. Subduction of the oceanic plate could have recycled a substantial amount of Hg from marine reservoirs into Earth's mantle. In the future, based on well-defined Hg-MIF signals in mantle-derived rocks and the subducted marine materials (e.g., sediments and seawater), the amount of marine Hg recycled into the mantle may be precisely quantified.

6. Conclusion

Lamprophyre samples in the study areas have the quality of enrichment of LREEs and depletion in HFSEs with remarkable Nb—Ta negative anomalies, suggesting the recycling of subducted marine sediments into the mantle. The observed positive Δ^{199}Hg in the studied lamprophyres suggests that Hg cycles at the Earth's surface and in interior reservoirs can be interconnected. Mercury in marine reservoirs (e.g., marine sediments and seawaters) may recycle into the Earth's crust and mantle through subduction processes. This study, therefore, verifies Hg isotopes may be used as a new tool for petrogenetic tracing, especially constraining the deep cycling of Hg on Earth.

Declaration of Competing Interest

The authors declare that they have no known competing financial interestsor personal relationships that could have appeared to influence the work reported in this paper.

Acknowledgment

This work was supported by the National Natural Science Foundation of China (41873047, 41673049, 42073047) and the Chinese Academy of Sciences through the Hundred Talent Plan to Runsheng Yin and Jing-Jing Zhu. Drs. Zhi-Kuan Qian from Guizhou Minzu University and Wei Gao from the Institute of Geochemistry, Chinese Academy of Sciences are thanked for their help during fieldwork.

Appendix A. Supplementary data

Supplementary data to this article can be found online at https://doi.org/10.1016/j.chemgeo.2021.120505.

References

Aghazadeh, M., Prelević, D., Badrzadeh, Z., Braschi, E., van den Bogaard, P., Conticelli, S., 2015. Geochemistry, Sr–Nd–Pb isotopes and geochronology of amphibole- and mica-bearing lamprophyres in northwestern Iran: Implications for mantle wedge heterogeneity in a palaeo-subduction zone. Lithos 216-217, 352–369.
Anderson, D.L., 2006. Speculations on the nature and cause of mantle heterogeneity. Tectonophysics 416 (1–4), 7–22.
Bergman, S.C., 1987. Lamproites and other potassium-rich igneous rocks: a review of their occurrence, mineralogy and geochemistry. Geol. Soc. London, Special Pub. 30 (1), 103–190.
Bergquist, B.A., Blum, J.D., 2007. Mass-dependent and-independent fractionation of Hg isotopes by photoreduction in aquatic systems. Science 318 (5849), 417–420.
Biswas, A., Blum, J.D., Keeler, G.J., 2008. Mercury storage in surface soils in a Central Washington forest and estimated release during the 2001 Rex Creek Fire. Sci. Total Environ. 404 (1), 129–138.
Blum, J.D., Bergquist, B.A., 2007. Reporting of variations in the natural isotopic composition of mercury. Anal. Bioanal. Chem. 388 (2), 353–359.
Blum, J.D., Sherman, L.S., Johnson, M.W., 2014. Mercury Isotopes in Earth and Environmental Sciences. Annu. Rev. Earth Planet. Sci. 42 (1), 249–269.
Canil, D., Crockford, P.W., Rossin, R., Telmer, K., 2015. Mercury in some arc crustal rocks and mantle peridotites and relevance to the moderately volatile element budget of the Earth. Chem. Geol. 396, 134–142.
Carignan, J., Estrade, N., Sonke, J.E., Donard, O.F., 2009. Odd isotope deficits in atmospheric Hg measured in lichens. Environ. Sci. Technol. 43 (15), 5660–5664.
Chen, M.H., Zhang, W., Yang, Z.X., Lu, G., Hou, K.J., Liu, J.H., 2009. Zircon SHRIMP U-Pb age and Hf isotopic composition of ultrabasic rock walls from white beds in Southwestern Guizhou. Mineral Deposits 03, 240–250.
Chen, J., Hintelmann, H., Feng, X., Dimock, B., 2012. Unusual fractionation of both odd and even mercury isotopes in precipitation from Peterborough, ON, Canada. Geochim. Cosmochim. Acta 90, 33–46.
Demers, J.D., Blum, J.D., Zak, D.R., 2013. Mercury isotopes in a forested ecosystem: Implications for air-surface exchange dynamics and the global mercury cycle. Glob. Biogeochem. Cycles 27 (1), 222–238.
Deng, C., Sun, G., Rong, Y., Sun, R., Sun, D., Lehmann, B., Yin, R., 2021. Recycling of mercury from the atmosphere-ocean system into volcanic-arc–associated epithermal gold systems. Geology 49 (3), 309–313.
Elliott, T., 2004. Tracers of the slab. In: Eiler, J. (Ed.), Inside the Subduction Factory, 238. American Geophysical Union Geophysical Monograph, pp. 23–45.
Geng, H., Yin, R., Li, X., 2018. An optimized protocol for high precision measurement of Hg isotopic compositions in samples with low concentrations of Hg using MC-ICP-MS. J. Anal. At. Spectrom. 33 (11), 1932–1940.
Grasby, S.E., Shen, W., Yin, R., Gleason, J.D., Blum, J.D., Lepak, R.F., Hurley, J.P., Beauchamp, B., 2017. Isotopic signatures of mercury contamination in latest Permian oceans. Geology 45 (1), 55–58.
Hauser, N., Matteini, M., Omarini, R.H., Pimentel, M.M., 2010. Constraints on metasomatized mantle under Central South America: evidence from Jurassic alkaline lamprophyre dykes from the Eastern Cordillera, NM Argentina. Mineral. Petrol. 100 (3–4), 153–184.
Hofmann, A.W., 2003. Sampling mantle heterogeneity through oceanic basalts: isotopes and trace elements. In: Carlson, R.W. (Ed.), Treatise on Geochemistry, 2, pp. 61–101.
Jiskra, M., Wiederhold, J.G., Skyllberg, U., Kronberg, R.M., Kretzschmar, R., 2017. Source tracing of natural organic matter bound mercury in boreal forest runoff with mercury stable isotopes. Environ Sci Process Impacts 19 (10), 1235–1248.
Kincaid, C., Druken, K.A., Griffiths, R.W., Stegman, D.R., 2013. Bifurcation of the Yellowstone plume driven by subduction-induced mantle flow. Nat. Geosci. 6 (5), 395–399.
Kwon, S.Y., Blum, J.D., Yin, R., Tsui, M.T.-K., Yang, Y.H., Choi, J.W., 2020. Mercury stable isotopes for monitoring the effectiveness of the Minamata Convention on Mercury. Earth Sci. Rev. 203, 103111.
Lenton, T.M., Crouch, M., Johnson, M., Pires, N., Dolan, L., 2012. First plants cooled the Ordovician. Nat. Geosci. 5 (2), 86–89.
Li, Q., Li, X., Wu, F., Liu, Y., Tabg, G., 2016. Accessary minerals SIMS U-Th-Pb dating for kimberlite and lamproite. Acta Geologica Sinica (English Edition) 90, 74–75.
Liu, S., Su, W., Hu, R., Feng, C., Gao, S., Coulson, I.M., Wang, T., Feng, G., Tao, Y., Xia, Y., 2010. Geochronological and geochemical constraints on the petrogenesis of alkaline ultramafic dykes from Southwest Guizhou Province, SW China. Lithos 114 (1–2), 253–264.
Lustrino, M., Agostini, S., Chalal, Y., Fedele, L., Stagno, V., Colombi, F., Bouguerra, A., 2016. Exotic lamproites or normal ultrapotassic rocks? The Late Miocene volcanic rocks from Kef Hahouner, NE Algeria, in the frame of the circum-Mediterranean lamproites. J. Volcanol. Geotherm. Res. 327, 539–553.
Moynier, F., Chen, J., Zhang, K., Cai, H., Wang, Z., Jackson, M.G., Day, J.M.D., 2020. Chondritic mercury isotopic composition of Earth and evidence for evaporative equilibrium degassing during the formation of eucrites. Earth Planet. Sci. Lett. 551, 116544.
Owen, J.P., 2008. Geochemistry of lamprophyres from the Western Alps, Italy: implications for the origin of an enriched isotopic component in the Italian mantle. Contrib. Mineral. Petrol. 155 (3), 341–362.
Pearce, J.A., Stern, R.J., Bloomer, S.H., Fryer, P., 2005. Geochemical mapping of the Mariana arc-basin system: implications for the nature and distribution of subduction components. Geochem. Geophys. Geosyst. 6 (7), Q07006.
Pirrone, N., Cinnirella, S., Feng, X., Finkelman, R.B., Friedli, H.R., Leaner, J., Mason, R., Mukherjee, A.B., Stracher, G., Streets, D.G., 2009. Global mercury emissions to the atmosphere from natural and anthropogenic sources, 10 (13), 5951–5964.
Rock, N.M.S., 1991. Lamprophyres, 285. Blackie and Son, Glasgow.

Selin, N.E., 2009. Global biogeochemical cycling of mercury: a review. Annu. Rev. Environ. Resour. 34 (1), 43–63.
Sherman, L.S., Blum, J.D., Nordstrom, D.K., McCleskey, R.B., Barkay, T., Vetriani, C., 2009. Mercury isotopic composition of hydrothermal systems in the Yellowstone Plateau volcanic field and Guaymas Basin sea-floor rift. Earth Planet. Sci. Lett. 279 (1–2), 86–96.
Smith, C.N., Kesler, S.E., Klaue, B., Blum, J.D., 2005. Mercury isotope fractionation in fossil hydrothermal systems. Geology 33 (10), 825–828.
Smith, C.N., Kesler, S.E., Blum, J.D., Rytuba, J.J., 2008. Isotope geochemistry of mercury in source rocks, mineral deposits and spring deposits of the California Coast Ranges, USA. Earth Planet. Sci. Lett. 269 (3–4), 399–407.
Stern, R.J., Tamura, Y., Masuda, H., Fryer, P., Martinez, F., Ishizuka, O., Bloomer, S.H., 2013. How the Mariana Volcanic Arc ends in the south. Island Arc 22 (1), 133–148.
Štrok, M., Baya, P.A., Hintelmann, H., 2015. The mercury isotope composition of Arctic coastal seawater. Compt. Rendus Geosci. 347 (7–8), 368–376.
Su, W.C., 2002. The Hydrothermal Fluid Geochemistry of the Carlin-type Gold Deposits in Southwestern Yangtze Craton, China. Unpublished Ph.D. Thesis. Institute of Geochemistry, Chinese Academy of Sciences, Guiyang, China (in Chinese with English Abstract).
Su, W.C., Hu, R., Xia, B., Xia, Y., Liu, Y., 2009. Calcite Sm-Nd isochron age of the Shuiyindong Carlin-type gold deposit, Guizhou, China. Chem. Geol. 258 (3–4), 269–274.
Su, H.M., Jiang, S.Y., Zhang, D.Y., Wu, X.K., 2017. Partial Melting of Subducted Sediments Produced early Mesozoic Calc-alkaline Lamprophyres from Northern Guangxi Province, South China. Sci. Rep. 7 (1), 4864.
Sun, S.-S., McDonough, W.-S., 1989. Chemical and isotopic systematics of oceanic basalts: implications for mantle composition and processes. Geol. Soc. London, Special Publications 42 (1), 313–345.
Williams, H.M., Turner, S.P., Pearce, J.A., Kelley, S.P., Harris, N.B.W., 2004. Nature of the source regions for post-collisional, potassic magmatism in Southern and Northern Tibet from geochemical variations and inverse trace element modelling. J. Petrol. 3, 555–607.
Winchester, J.A., Floyd, P.A., 1977. Geochemical discrimination of different magma series and their differentiation products using immobile elements. Chem. Geol. 20, 325–343.
Xiang, L., Zheng, J., Siebel, W., Griffin, W.L., Wang, W., O'Reilly, S.Y., Li, Y., Zhang, H., 2018. Unexposed Archean components and complex post-Archean accretion/reworking processes beneath the southern Yangtze Block revealed by zircon xenocrysts from the Paleozoic lamproites, South China. Precambrian Res. 316, 174–196.
Xiang, L., Zheng, J., Zhai, M., Siebel, W., 2020. Geochemical and Sr–Nd–Pb isotopic constraints on the origin and petrogenesis of Paleozoic lamproites in the southern Yangtze Block, South China. Contrib. Mineral. Petrol. 175 (4), 29.
Yin, R., Feng, X., Chen, B., Zhang, J., Wang, W., Li, X., 2015. Identifying the sources and processes of mercury in subtropical estuarine and ocean sediments using Hg isotopic composition. Environ. Sci. Technol. 49 (3), 1347–1355.
Yin, R., Feng, X., Hurley, J.P., Krabbenhoft, D.P., Lepak, R.F., Hu, R., Zhang, Q., Li, Z., Bi, X., 2016. Mercury isotopes as proxies to identify sources and environmental impacts of mercury in sphalerites. Sci. Rep. 6, 18686.
Yin, R., Xu, L., Lehmann, B., Lepak, R.F., Hurley, J.P., Mao, J., Feng, X., Hu, R., 2017. Anomalous mercury enrichment in early Cambrian black shales of South China: Mercury isotopes indicate a seawater source. Chem. Geol. 467, 159–167.
Yu, B., Fu, X., Yin, R., Zhang, H., Wang, X., Lin, C.J., Wu, C., Zhang, Y., He, N., Fu, P., Wang, Z., Shang, L., Sommar, J., Sonke, J.E., Maurice, L., Guinot, B., Feng, X., 2016. Isotopic composition of atmospheric mercury in china: new evidence for sources and transformation processes in air and in vegetation. Environ. Sci. Technol. 50 (17), 9262–9269.
Zambardi, T., Sonke, J.E., Toutain, J.P., Sortino, F., Shinohara, H., 2009. Mercury emissions and stable isotopic compositions at Vulcano Island (Italy). Earth Planet. Sci. Lett. 277 (1–2), 236–243.
Zerkle, A.L., Yin, R., Chen, C., Li, X., Izon, G.J., Grasby, S.E., 2020. Anomalous fractionation of mercury isotopes in the late Archean atmosphere. Nat. Commun. 11 (1), 1709.
Zheng, W., Hintelmann, H., 2009. Mercury isotope fractionation during photoreduction in natural water is controlled by its Hg/DOC ratio. Geochim. Cosmochim. Acta 73 (22), 6704–6715.
Zheng, W., Obrist, D., Weis, D., Bergquist, B.A., 2016. Mercury isotope compositions across north American forests. Glob. Biogeochem. Cycles 30 (10), 1475–1492.
Zhou, D., Zgabg, C., Liu, Y., 1998. Research on basic rock wall groups in the basement rock blocks of the continental orogenic belt-taking the wudeng block in Southern Qinling as an example. Adv. Earth Sci. (in Chinese) 02, 40–45.